Available online at www.sciencedirect.com
ScienceDirect
Journal of Electroanalytical Chemistry 601 (2007) 181–193
Journal of Electroanalytical Chemistry
www.elsevier.com/locate/jelechem

# Adsorption kinetic and properties of self-assembled monolayer based on mono(6-deoxy-6-mercapto)-β-cyclodextrin molecules

Flavio S. Damos, Rita C.S. Luz, Adão A. Sabino, Marcos N. Eberlin, Ronaldo A. Pilli, Lauro T. Kubota *

*Institute of Chemistry, UNICAMP, P.O. Box 6154, 13084-971 Campinas, SP, Brazil*

Received 12 June 2006; received in revised form 30 August 2006; accepted 13 November 2006
Available online 20 December 2006

**Abstract**

The kinetic of the assembly and adsorption processes of mono(6-deoxy-6-mercapto)-β-cyclodextrin (βCDSH) on gold surfaces in situ and in real time have been investigated by surface plasmon resonance technique (SPR). The film thickness, dielectric constant and its coverage capability were determined by SPR with one-wavelength approach. To unambiguously determine the film parameters avoiding multi-layer adsorption as well as an underestimation of the binding constants of the adsorption process, the influence of the mass transport of βCDSH was investigated and controlled. Under flow regime the SPR angle was monitored in several concentrations of thiol and the data were fitted by using a two-step adsorption model based on a fast adsorption of the thiol molecules in a first step followed by its slow rearrangement on the gold surface. Finally, the selectivity of the host–guest property of the βCDSH monolayer was investigated using $[Fe(CN)_6]^{3-/4-}$ and ferrocenemonocarboxylic acid as redox probes.


*Keywords:* Adsorption; Kinetics; Self-assembled monolayers; Cyclodextrin; Surface plasmon resonance

## 1. Introduction

Molecular recognition phenomena based on host–guest systems have attracted enormous research interest in nowadays [1]. By careful selection of host and guest molecules, specific properties of the resulting inclusion compounds can be targeted [2]. Inclusion of a guest without covalent binding into the host material can serve many purposes, such as solubility enhancement, protection against degradation by light, oxygen or removing undesired substances [3]. In supramolecular chemistry four systems have been extensively investigated: crown ethers, calixarenes, cyclophanes and cyclodextrins [4].

Among them, cyclodextrins (CDs) have been intriguing due to their unique physicochemical characteristics, including the formation of host–guest complexes with a wide variety of organic compounds, favorable aqueous solubility and extremely low toxicity against living systems [5]. As a result, the complexation by CDs is widely used in the pharmaceutical industry, food technology and agriculture [6]. Recently, the interest on surface bound CDs has increased significantly with the purpose to develop biomimetic and highly selective systems.

Therefore, numerous methods for immobilizing these molecules have been presented, including physical adsorption [7], self-assembed monolayers [8], polymeric films of CDs [9], plasticized membranes of lipophilic CDs [10] as well as immobilization of cyclodextrins within composites [11]. Among these methods, the self-assembling of cyclodextrins have attracted increasing interest, since it allows the CDs cavity to interact with guest molecules without interference of the matrix used for CDs immobilization (e.g. CDs immobilized in conducting polymers) [12,13]. When complexes matrices are used, it is difficult to determine if the binding constants taken in host–guest interaction studies are exclusively affected by the affinity of the

* Corresponding author. Tel.: +55 19 3788 3127; fax: +55 19 3788 3023.
*E-mail address:* kubota@iqm.unicamp.br (L.T. Kubota).

0022-0728/$ - see front matter © 2006 Elsevier B.V. All rights reserved.
doi:10.1016/j.jelechem.2006.11.004

cavity by the guest. Although the high interest on self-assembed monolayers (SAMs) of CDs, little efforts have been done to understand the assembling process of the modified cyclodextrins. Many models of adsorption, including Langmuiriam [12], diffusion-controlled Langmuir model [14], purely diffusion controlled adsorption [14], and second-order non-diffusion-limited model [15] have been applied in the kinetic investigation of the thiols adsorption. Each model has been shown to well-fitted the experimental data in a limited concentration range [14–16].

In addition, efforts have been done to effectively show that the SAM method to prepare β-cyclodextrin film does not block the ability of these host molecules to form inclusion complexes. We report herein an extensive investigation of the CD self-assembling process considering the adsorption, desorption as well as the rearrangement of these molecules on the gold surface by in situ and in real time surface plasmon resonance (SPR) measurements. The ability of the assembled CD to form inclusion complexes is also reported.

## 2. Experimental

### 2.1. Reagents and materials

All chemicals were of analytical grade; β-cyclodextrin used in this study was acquired from Merck (Darmstadt, Germany). Sulfuric acid ($H_2SO_4$) from Synth (São Paulo, Brazil), hydrogen peroxide ($H_2O_2$) from Merck (Darmstadt, Germany), 11-mercaptoundecanoic acid (95%) from Aldrich (Milwaukee, WI, USA), potassium ferrocyanide from J.T. Baker (Phillipsburg, NJ, USA), ferrocenemonocarboxylic acid from Sigma (St. Louis, MO, USA) and ethanol (99%) from Synth (São Paulo, Brazil) were used as received. The deionized water was used after being purified in a Milli Q system and the actual pH of the solutions was determined with a Corning pH/ion analyser 350 model. A gold sensor disk (used as working electrode) composed of a gold sensing surface (thickness of 50 nm) deposited onto a glass microscope slide using a titanium adhesion layer (thickness of 1.5 nm) was acquired from Xantec Bioanalytics (Muenster, Germany). The sensor disk was optically attached to the prism using an index-matching fluid $n_d$ (25 °C) = 1.518, Cargille Laboratories (Cedar Grove, NJ, USA).

### 2.2. Synthesis of the thiol modified cyclodextrin

#### 2.2.1. Mono(6-deoxy-6-p-tolylsulfonyl)-β-cyclodextrin [17]

A solution of NaOH (6.5 g, 162.5 mmol) in water (20 ml) was added drop wise over 6 min to a suspension of β-cyclodextrin (50 g, 44.05 mmol) in water (500 ml). The suspension became homogeneous and pale yellow before ending the addition. In the next step, a solution of *p*-toluenesulfonyl chloride (10 g, 52.38 mmol) dissolved in acetonitrile (30 ml) was drop wised over 8 min to this pale yellow solution, causing an immediate formation of a white precipitate. After stirring for 3 h at room temperature, the white precipitate was filtered off and the filtrate was stirred for 24 h at 4 °C. The precipitate formed was collected by suction, recrystallized in water successively to give 1.74 g (1.35 mmol, 3.5% yield) of a white precipitate. Formation of the desired product was confirmed by MALDI-TOF in the positive ion mode, which detected an ion of *m*/*z* 1311.09 for $[M + Na]^+$ as well as of *m*/*z* 1327.14 for $[M + K]^+$. Calculated for $C_{49}H_{76}O_{37}S$ from $[M + Na]^+$ was 1288.09 (Fig. 1a). $^1$H NMR (DMSO-d6): $\delta$ 2.42 (s, 3H), 3.10–3.45 (m, 14H), 3.45–3.70 (m, 28H), 4.10–4.60 (m, 6H), 4.76 (s, br, 2H), 4.83 (s, br, 5H), 5.60–5.85 (m, 14H), 7.42 (d, 2H, $J = 8.2$ Hz), 7.74 (d, 2H, $J = 8.2$ Hz) [18].

#### 2.2.2. Mono(6-deoxy-6-mercapto)-β-cyclodextrin [18]

A solution of mono(6-deoxy-6-*p*-tolylsulfonyl)-β-cyclodextrin (1.72 g, 1.34 mmol) above prepared and thiourea (1.72 g, 22.60 mmol) in a mixture of methanol-water (80%, v/v) was refluxed for 48 h. The volatiles were removed in a rotating evaporator and the solid residue was treated with methanol (30 ml) under stirring. The precipitate (isothiouronium salt) was filtered and washed with acetone.

The solid was dissolved in a solution of sodium disulfite (0.012 g, 0.063 mmol) in aqueous 1 mol $l^{-1}$ NaOH (10 ml) and stirred for 30 min at room temperature. The solution was acidified with 1 mol $l^{-1}$ HCl to pH 3 and then, trichloroethylene (0.5 ml) was added and the mixture was treated in ultrasonic bath for 10 min. The precipitate was filtered, recrystallized from cold water and dried to give a white precipitate (0.541 g, 0.47 mmol, 31.45% yield). Formation of the desired product has been confirmed by MALDI-TOF in the positive ion mode, which detected an ion of *m*/*z* 1173.30 for $[M + Na]^+$ as well as of *m*/*z* 1189.34 for $[M + K]^+$. Calculated for $C_{42}H_{70}O_{34}S$ from $[M + Na]^+$ was 1150.32 (Fig. 1b). $^1$H NMR (DMSO-d6): $\delta$ 2.01 (t, $J = 7.5$ Hz), 2.70 (m, 1H), 2.90 (m, 1H), 3.15–3.40 (m, 14 H), 3.40–3.80 (m, 26H), 3.40–4.40 (s, br, 20H). 4.76 (s, br, 7H); $^{13}$C NMR (DMSO-d6): $\delta$ 25.7, 59.9, 71.1, 72, 72.4, 72.8, 73.1, 81.5, 81.8, 84.1, 101.9, 102.2 [18].

### 2.3. Characterization by MALDI-TOF mass spectrometry

The determination of molar mass of modified cyclodextrin performed by MALDI-TOF mass spectrometry analyses were performed with a MALDI-TOF (Micromass/Waters) mass spectrometer. The samples were prepared by mixing 20 μl of the matrix solution (1% w/v 2,5-dihydroxybenzoic acid in water) with 1 μl of modified cyclodextrin solution (1% w/v in water) and 1 μl of this resulting solution was added to spots on the MALDI target plate and leave to dry on air before the analysis. The sample was ionized by nitrogen UV laser (337 nm) and the ions formed were accelerated with 15 kV potential in the flight tube. The mass spectra were acquired using the TOF (time of flight) mass analyzer working in the reflection mode.

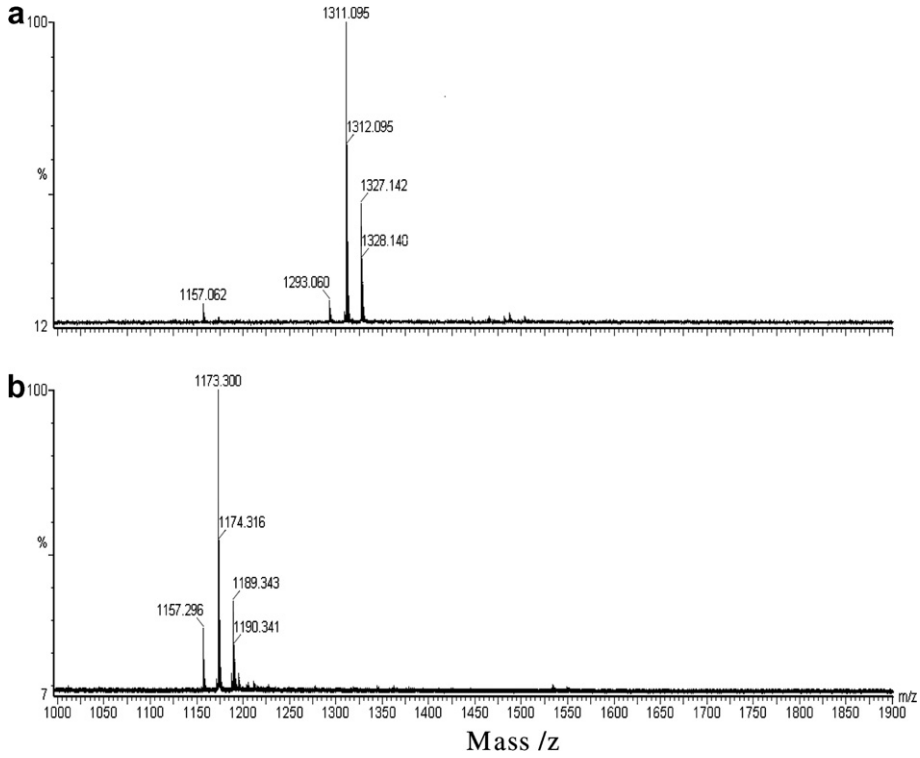


Fig. 1. MALDI-TOF spectra of mono(6-deoxy-6-*p*-tolylsulfonyl)-β-cyclodextrin (a) and mono(6-deoxi-6-mercapto)-β-cyclodextrin (b).

### 2.4. Surface plasmon resonance measurements

An ESPRIT instrument (Echo Chemie B.V., Ultrech, Netherlands) was used to perform the optical measurements of the SPR angle and cyclic voltammetry was carried out with a potentiostat (μAUTOLAB) from Echo Chemie (Ultrecht, Netherlands). The ESPRIT instrument is based on the Kretschmann configuration [19] with a scanning-angle setup. In this system, the intensity of the reflected light is minimum in the resonance angle. This angle can be measured over a range of 4° in this equipment by using a diode detector. The incidence angle was varied by using a vibrating mirror (rotating over an angle of 5° at 77 Hz in 13 ms), which directs p-polarized laser light onto a 1 mm × 2 mm spot of the sensor disk via hemicilindrical prism of BK7 glass. In each cycle the reflectivity curves were scanned on both forward and backward movements of the mirror. In this vibrating mirror set-up, the resolution was 1m°. The light source of the system is composed of the laser diode with emission wavelength of 670 nm. In the experiments, a gold sensor disk containing a hemicylinder was mounted into a precleaned SPR cuvette. The cuvette was made of Teflon® to be inert. The solutions were injected into the cuvette using a syringe with a stainless steel needle (Fig. 2).

The contamination on gold surface between the polymerization experiments was avoided adopting the previously reported procedure, based on chemical surface treatment [20]. In order to achieve the best accuracy of the measurements the temperature was kept constant (25 °C) using a cooled water recirculating bath RTE/7 model from Neslab (Thermo Electron Corporation, Netherlands). The refraction index of the bulk solution (ethanol/water, ethanol) was measured with an Abbe-refratometer (ATTO instruments Co, Hong Kong).

The following procedure was adopted to monitor the adsorption process in situ by SPR: after mounting the sensor disk in the cell, 200 μl of ethanol or ethanol/water solution was added into the cell. The SPR angle in pure solvent was recorded for 10 minutes to establish a stable baseline. After this, the pure solvent was removed from the cell and mono(6-deoxy-6-mercapto)-β-cyclodextrin ethanolic solution was added into the cell using a syringe pump coupled to the injection needle. Finally, the SPR angle was recorded continuously during the adsorption process of mono(6-deoxy-6-mercapto)-β-cyclodextrin. A drain controlled by peristaltic pump was used to control the volume of the solution in the cell.

### 2.5. Data analysis

For the thickness ($d_3$) and dielectric constant ($\varepsilon_3$) determination for fully formed films of mono(6-deoxy-6-mercapto)-β-cyclodextrin, the experiment was modeled as a system of four layer, and the Fresnel equations for this system were used as previously reported [21]. According to the Fresnel equation for the p-polarized light the value of the reflectivity of the light ($R(\theta)$) depends on the incident angle as presented [21]

$$R(\theta) = |r_{1,4}(\theta)|^2 \quad (1a)$$

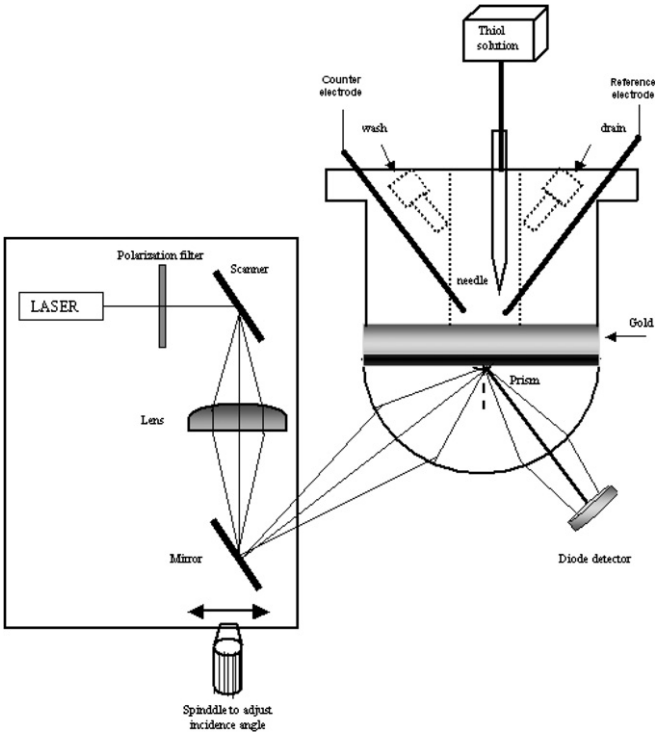


Fig. 2. Schematic diagram of the surface plasmon resonance spectroscopy using the Kretschmann configuration. The light source (LASER) of the SPR system is composed of the laser diode with the emission wavelength of 670 nm. A scanning mirror with a frequency of 76 Hz was used to obtain an angle scan of 4000 millidegrees (m°) in approximately 13 ms. A photodiode was used as a detector. The incidence angle of the light was adjusted by using a spindle to move the mirror position. The prism material was BK7. The gold disk was used as work electrode, a platinum wire as counter electrode and Ag/AgCl as reference electrode.

$$r_{i,4} = \frac{r_{i,i+1}(\theta) + r_{i+1,4}(\theta)\exp(2\mathrm{j}d_{i+1}k_{zi+1}(\theta))}{1 + r_{i,i+1}(\theta)r_{i+1,4}(\theta)\exp(2\mathrm{j}d_{i+1}k_{zi+1}(\theta))} \quad (1b)$$

where $(i = 2, 1;\ \mathrm{j} = \sqrt{-1})$, and

$$r_{i,i+1}(\theta) = \frac{\varsigma_{i+1}(\theta) - \varsigma_i(\theta)}{\varsigma_{i+1}(\theta) + \varsigma_i(\theta)} \quad (i = 1, 2, 3)$$

$$k_{zi}(\theta) = \frac{2\pi}{\lambda}\sqrt{\varepsilon_i - [(\omega/c)\sqrt{\varepsilon_0}\sin(\theta)]^2}$$

where $k_{zi}$ is the wavevector component perpendicular to the interface in the medium $i$ ($i = 1, 2, 3, 4$), $r_{i,i+1}$ represents the reflection ratio for the interface between the medium $i$ and $i + 1$, $\varepsilon_i$ ($i = 1, 2, 3, 4$) is the dielectric constant of the media, $d_i$ ($i = 2, 3$) represents the thickness of the gold and coating films and $\lambda$ represents the wavelength used during the measurements.

On the other hand, the dielectric constant of the gold film at the wavelength used (670 nm) was determined by using the Fresnel equation in a three-layer system experiment carried out for this purpose in a prism/gold layer/aqueous solution system. The Fresnel equations (Eq. (1)) describes the behavior of the reflectivity curves and it has been extensively used to extract optical information about thin films on metal surfaces by using some suppositions (such as suppose a known value of the film dielectric constant to extract its thickness) [22].

In this sense, it is impossible to determine simultaneously the refractive index and thickness of thin organic films on a metal surface by using one-color approach (using a single wavelength measurement) surface plasmon resonance, without implicating in a high uncertainty in the film thickness [22]. Thus, it was decided to use the methodology developed by Bruijn et al. [23] to find unequivocally the film thickness and its dielectric constant. In this sense, the following considerations were done on the Fresnel equation to simplify the relationship between the reflectivity and the incident angle: (a) only thin films should be considered as well as (b) it should be transparent such as its imaginary part of the dielectric constant become insignificant. As a result of these considerations, the Fresnel equations ((1a) and (1b)) were rewritten by considering the shift of the resonant wavenumber in the following form [24]:

$$\Delta k_{\min} = d_3\left(\frac{6.28}{\lambda}\right)^2 \frac{(\varepsilon_r\varepsilon_4)^{3/2}(\varepsilon_3 - \varepsilon_4)}{\varepsilon_3(\varepsilon_r - \varepsilon_4)^2} \quad (2)$$

where $\Delta k_{\min}$ represents the shift of the resonant wavenumber, $\varepsilon_4$ the dielectric constant of the bulk solution, $\varepsilon_3$ and $\varepsilon_r$ are the dielectric constant of the thin organic layer and real part of the dielectric constant of the gold layer, respectively, $\lambda$ and $d_3$ represents the used wavelength (670 nm) and the thickness of the organic layer.

From Eq. (2) the shift of the resonant wavenumber ($\Delta k_{\min}$) depends on five variables, including $\varepsilon_r$, $\varepsilon_4$, $\lambda$, $\varepsilon_3$ and $d_3$. The value of the refractive index of the bulk solution was determined as indicated in the experimental part of this work and the used laser diode emits wavelength of 670 nm. The value of real part of the dielectric constant of the gold layer ($\varepsilon_r = -11$) was determined as previously reported [20] with an error lower than 5%. In this sense, at least two equations are necessary to take the optical properties of the organic layer since two variables still remain unknown ($\varepsilon_3$ and $d_3$) in Eq. (2).

Three alternatives have been extensively used to solve this question: (1) multi-color approach, (2) two different metal surfaces and (3) multi-solvent approach. The former demands the knowledge of the value of the optical constant of the films for different wavelength used. On the other hand, the exchange of the metal implies to change the substrate used in the studies, which should result in changes of the affinities between the investigated layer and substrate (e.g. the interaction between a thiol film is different for gold when compared with the same study on silver) [24].

Based on these aspects, the drawbacks in the use of different values of $\varepsilon_r$ or $\lambda$ have created increasing interest for the multi-solvent approach. For this fixed wavelength method, two different solvents with two different dielectric constants, $\varepsilon_4(1)$ and $\varepsilon_4(2)$ are used to conduce two different measurements. Assuming that the structure of the film does not change, then clearly the two measured values $\Delta k_{\min}(1)$ and $\Delta k_{\min}(2)$ can be used to determine an unique set of

dielectric constant and film thickness, which can be verified by generating two expressions by using Eq. (2). By taken the ratio of these generated equations it can be verified that it is possible to determine unambiguously the value of the dielectric constant of the organic layer as follow:

$$\varepsilon_3 = \frac{\Delta k_{\min}(1)\varepsilon_4(2) - \alpha\Delta k_{\min}(2)\varepsilon_4(1)}{\Delta k_{\min}(1) - \alpha\Delta k_{\min}(2)} \quad (3a)$$

$$\text{where } \alpha = \left(\frac{\varepsilon_4(1)}{\varepsilon_4(2)}\right)^{3/2} \times \left[\frac{(\varepsilon_r - \varepsilon_4(1))^2}{(\varepsilon_r - \varepsilon_4(2))^2}\right] \quad (3b)$$

Thus, the film thickness and dielectric constant can be determined by introducing the value of the dielectric constant in Eq. (2). In practice, the dielectric constant and film thickness were determined by plotting three curves that describe all the possible dielectric constant-thickness pairs for each shift of the measured minimum reflectance. After the dielectric constant and thickness of the gold layer be controlled, the optical response of this system to the thiol film formation on solid surface could be determined.

## 3. Results and discussion

### 3.1. Dielectric constant and thickness for fully formed films of mono(6-deoxy-6-mercapto)-β-cyclodextrin (βCDSH)

The βCDSH adsorption was performed in an ethanol solution. The ethanol was chosen as solvent because the introduction of thiol group on the β-cyclodextrin molecule reduces its water solubility, as well to compare the kinetic data taken with those works reported in the literature due to the common use of this solvent in SAM investigations [25]. Thus, ethanol was used as a standard liquid ($\varepsilon_4 = 1.85$) and two binary solutions of ethanol/deionized water (75/25 $\varepsilon_4 = 1.83$ and 50/50 $\varepsilon_4 = 1.81$) were employed as the second and third media. These binary solutions were used because when a liquid with a significant different dielectric constant of the ethanol was used the angle range obtained using the scanning mirror was insufficient to probe the liquid exchange.

Six SPR spectra were recorded to determine dielectric constants and thickness of the mono(6-deoxy-6-mercapto)-β-cyclodextrin film. Initially, the SPR cuvette was filled with the ethanol solution and a SPR spectrum was obtained. After this step, the ethanol was changed by the first ethanol/water binary solution (75/25) and a new SPR curve was recorded. Finally, the second ethanol/water binary solution (50/50) was added in the measurement cell and the SPR curve was recorded again. Three reference spectra were, therefore, obtained for the comparison with the SPR curves for the prism/gold film/thiol film/liquid.

After obtaining the reference spectra for ethanol and binary solutions, the SPR cuvette was rinsed and filled with ethanol solution of βCDSH. The SPR angle was monitored during two hours. Finally, the SPR cuvette was intensively rinsed with ethanol and filled with it. SPR curve was recorded again and compared with the ethanol reference spectra (Fig. 3).

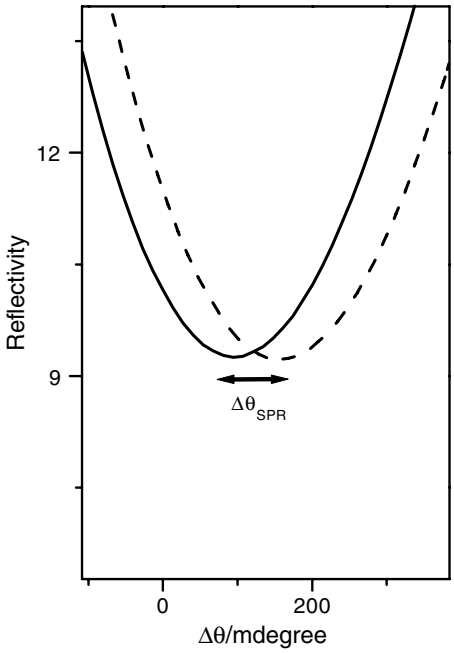


Fig. 3. SPR reflectivity curves for a clean gold surface in ethanol (solid line) and the same surface after the adsorption of βCDSH in ethanol solution (dashed line).

The last procedure was performed with the two binary solution and the variation of the SPR angle with and without βCDSH film was used to determine the shift of the minimum reflectance ($\Delta k_{\min}$) referent to the mono(6-deoxy-6-mercapto)-β-cyclodextrin film in ethanol as well as in relation to the binary solutions (75/25 and 50/50) obtaining respectively, 10,000, 12,000 and 14,000 $m^{-1}$ [24,25].

Using the shift values of the minimum reflectance ($\Delta k_{\min}$) in Eq. (2) as well as the values of $\varepsilon_r = -11$, $\varepsilon_1 = 2.30$ and $\varepsilon_4 = 1.85$ the thickness-dielectric constant pairs ($d_3, \varepsilon_3$) were calculated. Thus, for each value of $\Delta k_{\min}$ a curve making a variation of $\varepsilon_3$ from 1.9 up to 2.4 was plotted, since the commonly determined values of dielectric constants for several thiol organic films are in this range [26]. Therefore, one curve ($d_3$ versus $\varepsilon_3$) was obtained when ethanol was used as solvent (Fig. 4, solid line), one for the binary solution (75/25) (Fig. 4, dashed line) and another for the binary solution (50/50) (Fig. 4, dotted line).

An intersection point is found for the curves of the ethanol and binary solutions indicating the true values of $d_3$ and $\varepsilon_3$ as expected from Eq. (3). This intersection point represents the true thickness of the thiol film and the average dielectric constant for the fully formed βCDSH film after two hours. As a result, a dielectric constant of 2.0 and a thickness for βCDSH film of 12 Å were obtained, after exposing a gold film for two hours in a 0.5 mmol $l^{-1}$ βCDSH ethanol solution and following the rinsing process. An important point to be emphasized is that the thickness taken here for the βCDSH ultrathin films was smaller than

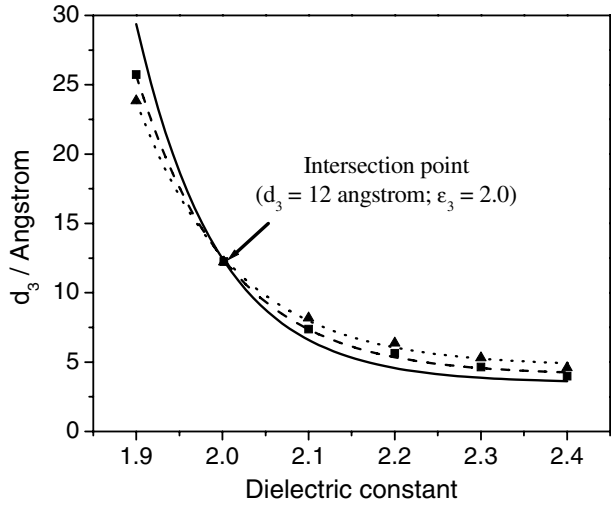


Fig. 4. Dielectric constants and thickness of the mono(6-deoxy-6-mercapto)-β-cyclodextrin film obtained from SPR spectra. Each curve represents a series of film thickness and dielectric constants when the ethanol (solid line), and the binary ethanol/deionized water (75/25 dashed line) and (50/50 dotted line) were used.

that expected for a closed packing of perpendicular aligned tori ($d_3 \sim 15.3$ A) and higher than an aligned monolayer in a cyclodextrin tori hexagonal closed packing parallel to the surface ($d_3 \sim 7.8$ A) which can be associated with the reminiscent physisorbed molecules at the first monolayer chemisorbed at the gold surface or the intermediate value of the thickness found as a result of a tilt of the cyclodextrin tori [1]. In order to obtain more detailed information about the assembly of these molecules on the gold surface, kinetics studies of the adsorption on the gold surface were performed with and without flow conditions of the adsorption processes.

### 3.2. Measurement of mono(6-deoxy-6-mercapto)-β-cyclodextrin adsorption kinetic

The relative thickness of the βCDSH film was determined using the dielectric constant obtained in the early experiments ($\varepsilon_3 = 2.0$) for a fully formed film. During the adsorption process, βCDSH molecules produce a partially formed monolayer (discontinue film), where the dielectric constant of the film varies from that observed for pure ethanol (1.85) to that fully formed monolayer (2.0). A simplified approach to deal this discontinuous film is the use of the Maxwell Garnett theory [27]. Such inhomogeneous system can be then proved to be equivalent to a homogeneous system with an effective dielectric constant ($\varepsilon_{\text{eff}}$) given by Eq. (4)

$$\varepsilon_{\text{eff}} = \varepsilon_4 \frac{\left(1 + 2q\left(\frac{(\varepsilon_3 - \varepsilon_4)}{(\varepsilon_3 + 2\varepsilon_4)}\right)\right)}{\left(1 - q\left(\frac{(\varepsilon_3 - \varepsilon_4)}{(\varepsilon_3 + 2\varepsilon_4)}\right)\right)} \tag{4}$$

where $q$ is the volume fraction (surface coverage) occupied by βCDSH, $\varepsilon_3$ and $\varepsilon_4$ are the dielectric constants of the fully formed βCDSH film and ambient solution, respectively. Considering the kinetics data for an unambiguous interpretation, the SPR angle was converted to relative thickness. Thus, the surface coverage could be interpreted in terms of film thickness variation or effective dielectric constant change as previously reported [20].

The change of the surface coverage can be correlated with the relative film thickness, as expected and the average thickness of the thiol film was used with the following relationship: $d_{3(\text{relative})} = q d_{3(\text{fully formed film})}$ ($q$ is the surface coverage, $d_{3(\text{relative})}$ is the average film thickness and $d_{3(\text{fully formed film})}$ is the final film thickness) where $q$ was taken as $\Delta\theta/\Delta\theta_{(\text{fully formed film})}$. $\Delta\theta$ is the SPR angle shift at time ($t$) function and $\Delta\theta_{(\text{fully formed film})}$ the SPR angle shift for the fully formed film.

Thus, the average thickness of the film was estimated and the dielectric constant determined for a full monolayer of mono(6-deoxy-6-mercapto)-β-cyclodextrin. The adsorption of the thiol on the gold substrate from its ethanolic solution was monitored in situ at time function. In order to warrant a complete adsorption of thiol, a high βCDSH concentration (500 μmol $l^{-1}$) was used [28,29].

As can be observed in Fig. 5, the values found for the film thickness are higher than that expected for a βCDSH monolayer, either in a closely aligned monolayer of cyclodextrin tori in a hexagonal closed packing parallel to the surface or closely packing of perpendicular aligned cyclodextrin molecules [1] which can be resulted from the presence of physisorbed molecules. Thus, the multilayer thiol adsorption process was considered as the reason of the high thickness verified values.

In order to consider the multilayer formation of βCDSH on the gold substrate was assumed that a first layer formed

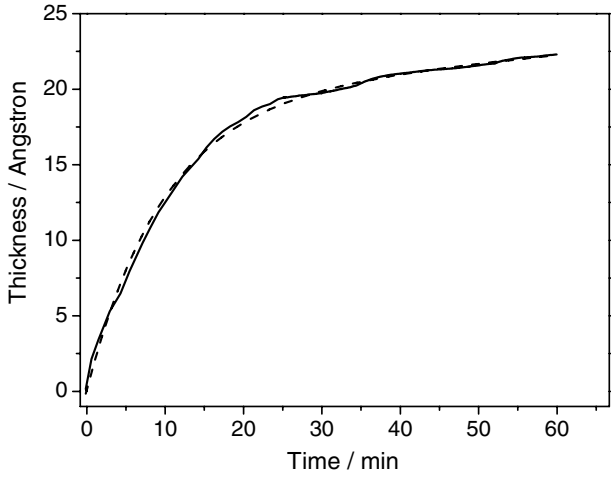


Fig. 5. Adsorption of mono(6-deoxy-6-mercapto)β-cyclodextrin from a 500 μmol $l^{-1}$ thiol ethanolic solution under hydrostatic conditions (solid line). The dashed line represents the curve calculated from the multilayer model which well adjusts to the experimental curve resulting in a non-linear regression coefficient of 0.9938 and a also a non-linear chi-square of 0.0208.

on the gold adsorption sites (Au) and, then, a second layer is pilled up on it as depicted in Eqs. (5a) and (5b):

$$A + Au \underset{k_{d1}}{\overset{k_{a1}}{\rightleftarrows}} A_1\text{–}Au \tag{5a}$$

$$A + A_1\text{–}Au \underset{k_{d2}}{\overset{k_{a2}}{\rightleftarrows}} A_2A_1\text{–}Au \tag{5b}$$

where A represents the adsorbate (βCDSH), $A_1$ and $A_2$ are the adsorbate in the first and second layer. Considering that, $k_{a1}$ and $k_{d1}$ represents the rate constant of adsorption and desorption of the first step (referring to first layer), respectively, and those corresponding to the second layer are denoted by $k_{a2}$ and $k_{d2}$, the adsorption rate equations in its differential form can be represented by:

$$\frac{d\theta_1}{dt} = k_{a1}C - (k_{a1}C + k_{d1})\theta_1 + k_{d1}\theta_2 \tag{6a}$$

and

$$\frac{d\theta_2}{dt} = k_{a2}C\theta_1 - (k_{a2}C + k_{d2})\theta_2 \tag{6b}$$

where $\theta_1$ represents the coverage associated with the first monolayer and become an expression of the number of adsorption sites occupied as a result of the formation of the first layer, $\theta_2$ is associated with the formation of the second layer, $\theta$ is the coverage associated with the total number of adsorption sites occupied for the assembly process $(\theta_1 + \theta_2)$ and $C$ is the βCDSH concentration. Integrating Eqs. (6a) and (6b) yields the time course of the multilayer formation for the first and second steps

$$\theta_1 = \left[\frac{(k_{a2}+k_{d2})k_{a1}C}{k_{obs,1}k_{obs,2}}\right] + \left[\frac{k_{a1}C}{k_{obs,1}-k_{obs,2}}\right] \times \left\{\left[\frac{(k_{a2}C+k_{d2})-k_{obs,1}}{k_{obs,1}}\right]\exp(-k_{obs,1}t) - \left[\frac{(k_{a2}C+k_{d2})-k_{obs,2}}{k_{obs,2}}\right]\exp(-k_{obs,2}t)\right\} \tag{7a}$$

$$\theta_2 = \left[\frac{k_{d2}Ck_{a1}C}{k_{obs,1}k_{obs,2}}\right] + \left[\frac{k_{a1}C}{k_{obs,1}-k_{obs,2}}\right] \times \left\{\left[\frac{(k_{a2}C)}{k_{obs,1}}\right]\exp(-k_{obs,1}t) - \left[\frac{k_{a2}C}{k_{obs,2}}\right]\exp(-k_{obs,2}t)\right\} \tag{7b}$$

and

$$\theta = \left\{\left[\frac{-k_{a1}C}{k_{obs,1}-k_{obs,2}}\right]\left[\frac{(k_{a2}C+k_{d2})+k_{a2}C-k_{obs,1}}{k_{obs,1}}\right][1-\exp(-k_{obs,1}t)]\right\} + \left\{\left[\frac{-k_{a1}C}{k_{obs,1}-k_{obs,2}}\right]\left[\frac{(k_{a2}C+k_{d2})+k_{a2}C-k_{obs,2}}{k_{obs,2}}\right][1-\exp(-k_{obs,2}t)]\right\} \tag{7c}$$

where

$$k_{obs,1} = \frac{k_{a1}C+k_{d1}+k_{a2}C+k_{d2}}{2} + \sqrt{\left(\frac{k_{a1}C+k_{d1}+k_{a2}C+k_{d2}}{2}\right)^2 - (k_{a1}k_{a2}C^2 + k_{a1}k_{d2}C + k_{d1}k_{d2})} \tag{8a}$$

$$k_{obs,2} = \frac{k_{a1}C+k_{d1}+k_{a2}C+k_{d2}}{2} - \sqrt{\left(\frac{k_{a1}C+k_{d1}+k_{a2}C+k_{d2}}{2}\right)^2 - (k_{a1}k_{a2}C^2 + k_{a1}k_{d2}C + k_{d1}k_{d2})} \tag{8b}$$

Thus, the curve referring to the adsorption of mono(6-deoxy-6-mercapto)-β-cyclodextrin obtained was fitted using Eq. (7c) in order to obtain the values of $k_{obs,1}$ and $k_{obs,2}$ by using non-linear curve fitting according to the specified model (Fig. 5, dashed line). Although a good fit was obtained of the theoretical model to the experimental data, the obtained values for $k_{obs,1}$ ($0.00017\ s^{-1}$) was lower than that expected for a single Langmuiriam process for thiol molecules adsorption as predicted by the first step of the proposed multilayer adsorption model (Eq. (5a)) [20].

Considering that the rate constants for thiol binding reaction should be very high as a result of the high affinity of the thiol to the gold surface [20], and the apparent rate constant ($k_{obs,1}$) obtained through the analysis of the SPR data is in the range of the molecules transport rate constant [30], it might be suspected that the binding and dissociation of molecules at the sensor surface may be limited by the mass transport to the sensor surface and the model become inadequate to found directly the binding and dissociation constants. Indeed, an anomalous high thickness values taken under non-flow conditions can be attributed to the molecules at the surface that are physisorbed on top of the monolayer, which do not occur under flow condition as verified to other thiol molecules [30].

The mass-transport effects on the kinetic parameters of the binding event (βCDSH adsorption) can be verified by the plots presented in Fig. 6. The first stage of the adsorption process (monitoring time: from 0 up to 10 min) was analyzed with the expression of a single Langmuiriam kinetic process

$$d\theta_1\, dt^{-1} = k_a C\theta_{max} - (k_a C + k_d)\theta_1 \tag{9}$$

where $\theta_{max}$ represents the maximum coverage taken during the first step of adsorption and $\theta_1$ the surface coverage taken at time ($t$), $k_a$ and $k_d$ represents the association and dissociation constants and $C$ the thiol concentration.

According to the predicted by Eq. (9), under non-limited mass transport conditions the first step should present a linear behavior in the plots of $d\theta_1\, dt^{-1}$ versus $\theta_1$. However, under non-flow condition the plot presents a region where the plotted line is independent of the variable $\theta_1$, which is well known to indicate that under these conditions the adsorption is diffusion controlled and no kinetic information of the binding process is available [32]. Therefore, further adsorption experiments were carried out under flow conditions.

Considering a simple Langmuirian process under kinetic control without influence of the multilayer processes, the

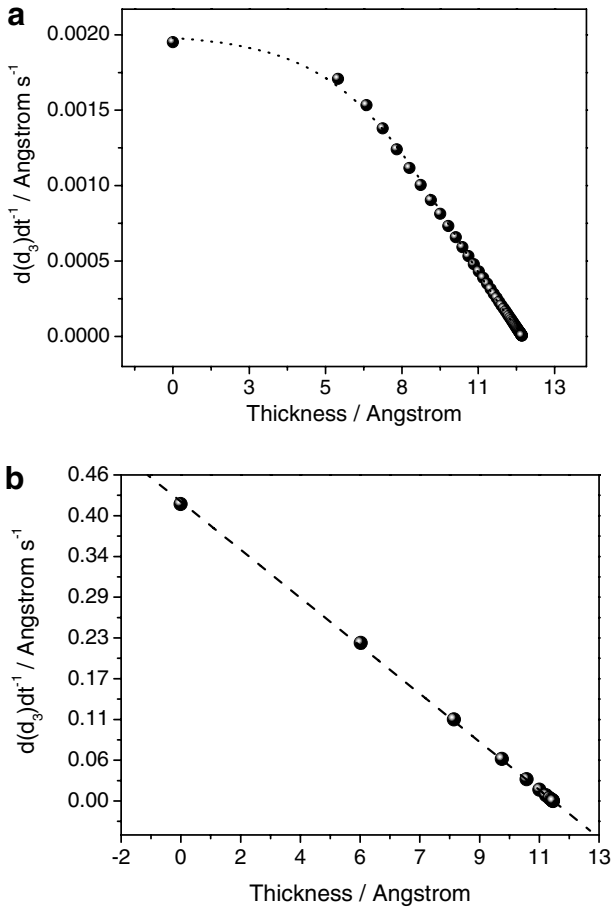


Fig. 6. Lines obtained from the association phase of Fig. 5 transformed into plots of $d(d_3)dt^{-1}$ versus $d_3$: (a) non-flow and (b) flow rate 30 μl $s^{-1}$.

thiol adsorption process was modeled based on two-step adsorption process based on a first rapid thiol adsorption followed by the molecule reorganization to form an assembled monolayer. Then, it is assumed that thiols molecules adsorbed in the first step can be desorbed and/or rearranged to form a perfect monolayer as depicted in Eqs. (10a) and (10b)

$$\mathrm{A} + \mathrm{Au} \underset{k_d}{\overset{k_a}{\rightleftarrows}} \mathrm{A_i}\text{–}\mathrm{Au}, \tag{10a}$$

$$\mathrm{A_i}\text{–}\mathrm{Au} \xrightarrow{k_t} \mathrm{A_r}\text{–}\mathrm{Au}, \tag{10b}$$

where A represents the adsorbate, Au is the adsorption site, $A_i$ represent the initially adsorbed species and $A_r$ is the rearranged species on the Au surface. If $k_a$ and $k_d$ denote the rate constants of association and dissociation and $k_t$ is the rate constant for thiol rearrangement during the second step of adsorption, the adsorption rate equations can be represented by Eqs. (11a) and (11b)

$$\frac{d\theta_1}{dt} = k_a C - (k_a C + k_d + k_t)\theta_1 - k_a C\theta_2 \tag{11a}$$

and

$$\frac{d\theta_2}{dt} = k_t \theta_1 \tag{11b}$$

where $\theta_1$ is the coverage in the first stage of the adsorption, $\theta_2$ represents the coverage for an assembled monolayer, $\theta$ is the coverage for overall adsorption process and $C$ is the adsorbate concentration. Integrating Eqs. (11a) and (11b) yields the time course of the monolayer formation for the first and second steps (details in supplementary material). Thus,

$$\theta_1 = \frac{-k_a C}{k_{obs,1} - k_{obs,2}}[\exp(-k_{obs,1}t) - \exp(-k_{obs,2}t)] \tag{12a}$$

$$\theta_2 = \frac{-k_a C}{k_{obs,1} - k_{obs,2}}\left\{\frac{k_t}{k_{obs,1}}[1 - \exp(-k_{obs,1}t)] - \frac{k_t}{k_{obs,2}}[1 - \exp(-k_{obs,2}t)]\right\} \tag{12b}$$

and

$$\theta = \frac{-k_a C(k_t - k_{obs,1})}{(k_{obs,1} - k_{obs,2})k_{obs,1}}[1 - \exp(-k_{obs,1}t)] + \frac{-k_a C(k_t - k_{obs,2})}{(k_{obs,1} - k_{obs,2})k_{obs,2}}[1 - \exp(-k_{obs,2}t)] \tag{12c}$$

where

$$k_{obs,1} = \frac{k_a C + k_d + k_t}{2} + \sqrt{\left(\frac{k_a C + k_d + k_t}{2}\right)^2 - k_a k_t C} \tag{13a}$$

$$k_{obs,2} = \frac{k_a C + k_d + k_t}{2} - \sqrt{\left(\frac{k_a C + k_d + k_t}{2}\right)^2 - k_a k_t C} \tag{13b}$$

The obtained raw data were fitted under flow conditions using Eq. (12c) and the result can be observed in Fig. 7 of a representative scan of the thiol adsorption from 500 μmol $l^{-1}$ βCDSH ethanol solution. The values of $k_{obs,1}$

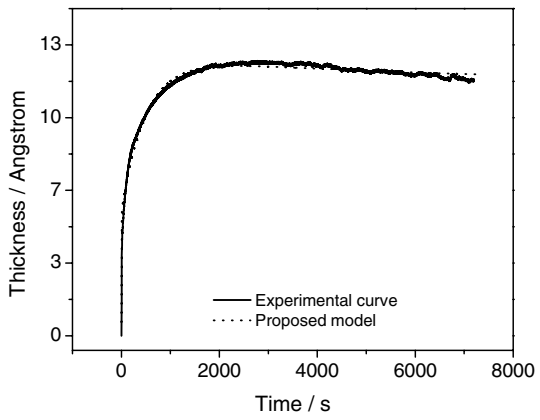


Fig. 7. Adsorption of mono(6-deoxy-6-mercapto)-β-cyclodextrin from an ethanol solution of 500 μmol $l^{-1}$ of the thiol (solid line). The dot line represents the curve calculated from rearrange-limited Langmuir model.

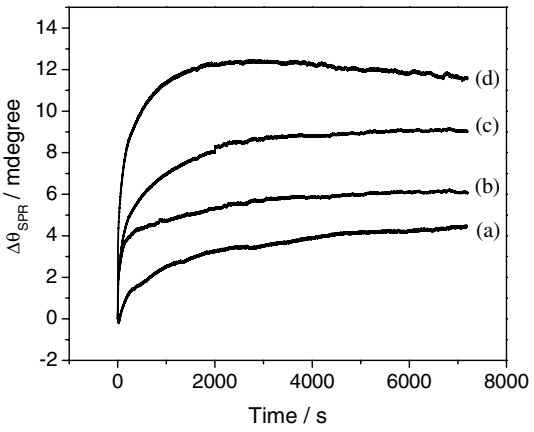


Fig. 8. Adsorption of βCDSH from ethanol on gold at different concentrations: (a) 1 μmol $l^{-1}$, (b) 10 μmol $l^{-1}$, (c) 100 μmol $l^{-1}$, (d) 500 μmol $l^{-1}$.

and $k_{obs,2}$ were obtained from the nonlinear curve fitting used according to the specified models. Indeed, the proposed model well-adjusts with the experimental data.

Fig. 8 shows the kinetics of the adsorption process for mono(6-deoxy-6-mercapto)-β-cyclodextrin at different concentrations. The average thickness was obtained using four different solutions (1 μmol $l^{-1}$, 10 μmol $l^{-1}$, 100 μmol $l^{-1}$ and 500 μmol $l^{-1}$). From the layer thickness versus time curves, at least two-time constants can be discerned.

The full monolayer coverage was only obtained in concentrations of 500 mmol $l^{-1}$ within two hours of adsorption process with a maximum thickness of 12 Å according to the previously determined value, indicating the formation of one monolayer [31]. Subsequently, the influence of the βCDSH concentration on the adsorption kinetics was evaluated using the rearrange-limited Langmuir adsorption model for all used concentration range. Table 1 presents the results of these fits.

This model does not assume a simple relationship between the $k_{obs}$ values and the thiol concentration like in a simple Langmuir model. The sum and the multiplication of $k_{obs,1}$ and $k_{obs,2}$ result in two relationship between obtained $k_{obs}$ and the thiol concentration as described by Eqs. (14a) and (14b)

$$k_{obs,1} + k_{obs,2} = k_a C + k_d + k_t \tag{14a}$$

and

$$k_{obs,1} k_{obs,2} = k_a k_t C \tag{14b}$$

Table 1
Values of $k_{obs,1}$ and $k_{obs,2}$ determined from raw data as a function of mono(6-deoxy-6-mercapto)-β-cyclodextrin concentration

| [βCDSH] (μmol $l^{-1}$) | $k_{obs,1}$ ($s^{-1}$) | $k_{obs,2}$ ($s^{-1}$) |
|---|---|---|
| 1 | 0.0027 ± (0.0015) | 0.00032 ± (0.0002) |
| 10 | 0.0029 ± (0.0008) | 0.0005 ± (0.0002) |
| 50 | 0.0058 ± (0.0009) | 0.0015 ± (0.0005) |
| 100 | 0.0089 ± (0.001) | 0.0017 ± (0.0007) |
| 500 | 0.035 ± (0.002) | 0.0022 ± (0.0009) |

In this sense, a plot of $k_{obs,1} + k_{obs,2}$ versus $C$ for a series of βCDSH concentrations gives a straight line with a slope equal to $k_a$ and an intercept of $k_d + k_t$. Similarly, a plot of $k_{obs,1}k_{obs,2}$ versus $C$ for the same concentrations also gives a straight line with a slope $k_a k_t$ (data not shown).

By combining the slope and intercepts taken for sum and multiplication of $k_{obs,1}$ and $k_{obs,2}$ values for $k_a$, $k_d$ and $k_t$ of 69 (±1) l $mol^{-1}$ $s^{-1}$, 0.00039 (±0.00005) $s^{-1}$ and 0.0023 (±0.0004) $s^{-1}$ were obtained, respectively. Based on these results, it is possible to assume that many molecules are adsorbed at an initial stage and then are rearranged to form a monolayer following the proposed model. In addition, the monolayer would be formed in the equilibrium state, where the excess of the molecules must be desorbed and assembled during the rearrangement. Thus, a dynamic and reversible adsorption process is part of the mechanism for attaining the adsorption equilibrium maximizing the packing density.

In order to corroborate the Langmuiriam process for βCDSH adsorption in the first step the line referring to the cyclodextrin adsorption was fitted as an Elovich kinetic [32] in the region of the first step of adsorption process. As is well known, the Elovich rate behavior (Eqs. (15a) and (15b)) takes into account that the adsorbate needs to overcome an energy barrier before binding such as

$$\frac{d\theta}{dt} = \frac{1}{\tau}(1-\theta)\exp\left(-\frac{\alpha\theta}{RT}\right) \tag{15a}$$

or in its integrated form as a time ($t$) function,

$$\theta(t) = \theta_{mono}\left[1 - \exp\left(\frac{t}{\tau}\right)^{\exp(-\alpha/RT)}\right] \tag{15b}$$

where $\tau$ is the time constant of the adsorption process, which become similar to the apparent kinetic rate constant before mentioned, $\alpha$ represents the maximum activation energy that the molecule has to overcome for binding, $R$ the gas constant, $T$ the absolute temperature and $\theta_{mono}$ the surface concentration of maximum coverage.

As a result of the fitting process was verified a $\alpha = 0$, which is the limit for the Elovich kinetic behavior as a Langmuiriam adsorption kinetic [33]. After the control of the thiol adsorption and assembling process the permselectivity of the film was investigated electrochemically to warrant the previously determined maximum surface coverage.

### 3.3. Electrochemical behavior of the mono(6-deoxy-6-mercapto)-β-cyclodextrin film toward $[Fe(CN)_6]^{3-/4-}$ and ferrocenemonocarboxylic acid ($FeCO_2H$)

As earlier presented, the dielectric constant of the formed self-assembled monolayer of mono(6-deoxy-6-mercapto)-β-cyclodextrin was lower than that expected for a perfect packing of adsorbed molecules ($\varepsilon_3 = 2.25$) [34] indicating an imperfect coverage of the surface. Hence, to estimate the surface coverage ($q$) of the film, the determined dielectric constant ($\varepsilon_3 = 2.0$) was considered in Eq. (4) as

an effective dielectric constant resulting in a $q$ of 0.62. Therefore, the use of a gold surface modified only with βCDSH can not be directly used successfully to construct size-selective films, since this film presents defects where the guest molecules could permeate to reach the electrode surface prejudicing the electrode selectivity.

In order to fill up the exposed surface between the cyclodextrin molecules (about of 40% of the surface) 11-mercaptoundecanoic acid (MUA) molecules were used, since they have been shown to promote full block of electron transfer of electrochemical probes [35]. Thus, the βCDSH-modified gold surface was immersed in a MUA ethanolic solution to promote fully coverage of the electrode surface. In order to verify the efficiency of the MUA molecule in filling up the defects in the SAM of βCDSH, the permselectivity of different monolayers was investigated by using the redox switching of the $[Fe(CN)_6]^{3-/4-}$ and $FeCO_2H$ as redox probes on bare electrode (curve 1), MUA monolayer (curve 2), (βCDSH) monolayer (curve 3) and mixed MUA/βCDSH monolayer (curve 4) modified electrodes.

Fig. 9(a) shows cyclic voltammograms for $[Fe(CN)_6]^{3-/4-}$ for gold electrode modified with several kinds of films and Fig. 10(a) shows the schematic representation of the interaction between the self-assembled monolayer and this electrochemical probe. The gold electrode modified with a mixed MUA/βCDSH monolayer (Fig. 9a, curve 4) presents no peaks referring to the oxidation or reduction couple. This behavior is expected to ferricyanide because its size is larger than the cavity of the β-cyclodextrin, and is also highly charged being impossible to be included in its cavity, thus the access of the probe to the gold electrode is efficiently blocked by the mixed monolayer as well as MUA monolayer (Fig. 10a, Scheme 2) [36].

The layer density or permeability of SAMs was evaluated in terms of available electrode surface ($\phi$) by considering the ratio between the oxidation peak current measured at the modified electrode and the peak current taken at the bare electrode, which yields the $\phi$ value [37] according to the well known microarray model for pinholes in self-assembled monolayers [38]:

$$\phi = i_{pa}(\text{cyclodextrin modified electrode})/i_{pa}(\text{bare gold electrode}) \quad (16)$$

Fig. 9(a), curve 3 gives a $\phi$ value of 0.65, which is in accordance to that obtained by SPR (0.62). The ability of the constructed films of βCDSH to include guest molecules from solution was investigated by the interaction of the βCDSH monolayer with $FeCO_2H$ chosen as the probe molecule due to its well known capacity to form inclusion complexes with β-cyclodextrin [39]. Cyclic voltammograms of $FeCO_2H$ on the gold electrode modified with mono(6-deoxy-6-mercapto)-β-cyclodextrin only (Fig. 9b, curve 3) shows that the oxidation and reduction peak currents is slightly affected when compared with those obtained at the bare gold electrode.

Since βCDSH promotes no barrier to this electrochemical probe, the access to the electrode surface is done through the defects on the cyclodextrin monolayer as well as across its cavity on the gold surface (Fig. 10(a), Scheme 3). Therefore, the cyclodextrin monolayer does not promote the suppression of the ferrocenemonocarboxylic acid redox processes (Fig. 9(b), curve 3) showing that it is possible to construct selective systems based on this mixed monolayer film.

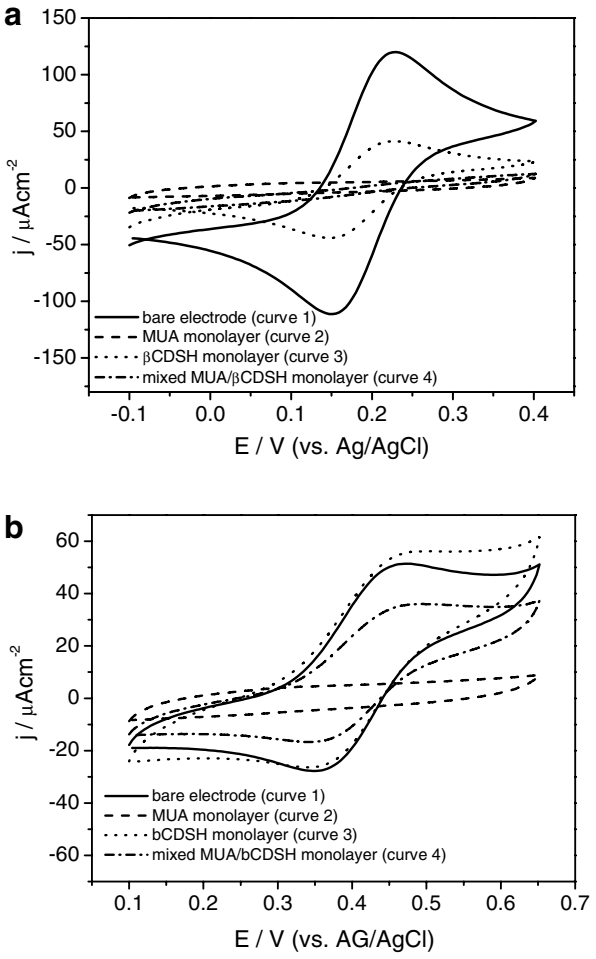


Fig. 9. (a) Cyclic voltammograms in 1 mmol $l^{-1}$ $K_3[Fe(CN)_6]$ containing 0.1 mol $l^{-1}$ KCl solution of a bare (1) and modified gold electrode with films of MUA (2), βCDSH (3) and mixed monolayer of MUA/βCDSH (4). (b) Cyclic voltammograms in 1 mmol $l^{-1}$ ferrocenemonocarboxylic acid containing 0.1 mol $l^{-1}$ KCl ethanolic solution (ethanol/water 50/50, v/v) of a bare (1) and modified gold electrode with films of MUA (2), βCDSH (3) and mixed monolayer of MUA/βCDSH (4).

In order to verify the capability of the cyclodextrin films to form inclusion complexes with the $FeCO_2H$ molecules on the electrode surface, the voltammetric experiments were performed immersing the mixed-monolayer modified electrode in the diluted $FeCO_2H$ ($10^{-6}$ M) ethanolic solution, washed and transferred to the supporting electrolyte solution to record the voltammogram. Fig. 11 shows the voltammograms recorded with cyclodextrin modified electrode, which presents a clear redox couple attributed to ferrocenemonocarboxylic acid into its cavity (full line) is observed.

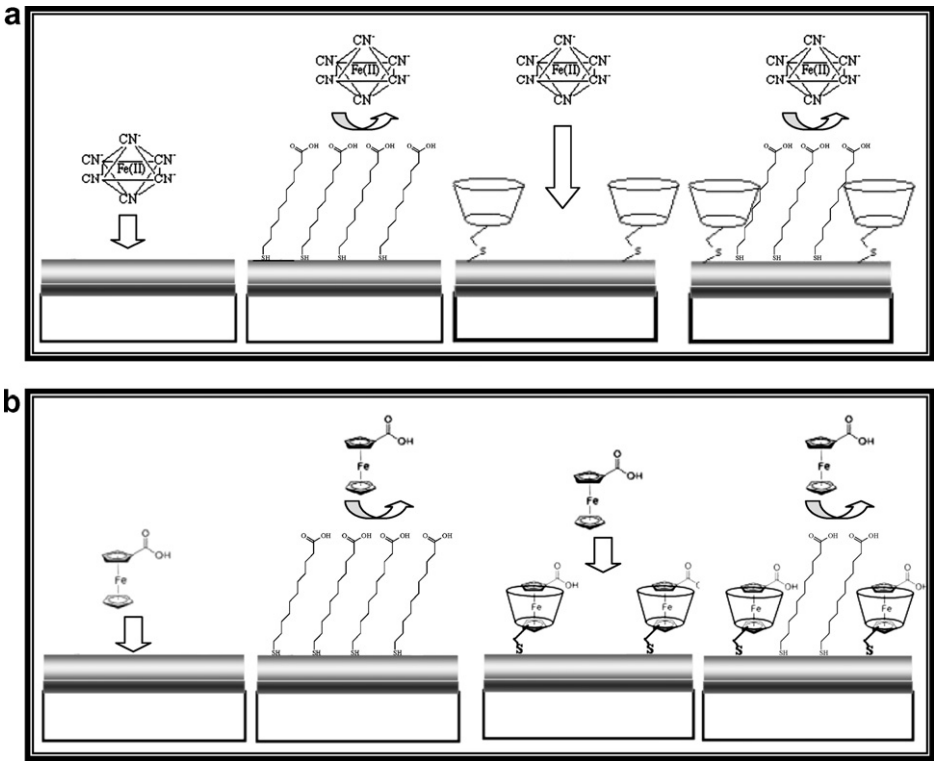


Fig. 10. Schematic diagram referring to the $[Fe(CN)_6]^{3-}$ (a) and ferrocenemonocarboxylic acid (b) interaction with: (1) bare electrode, (2) MUA monolayer, (3) βCDSH monolayer and (4) mixed MUA/βCDSH monolayer.

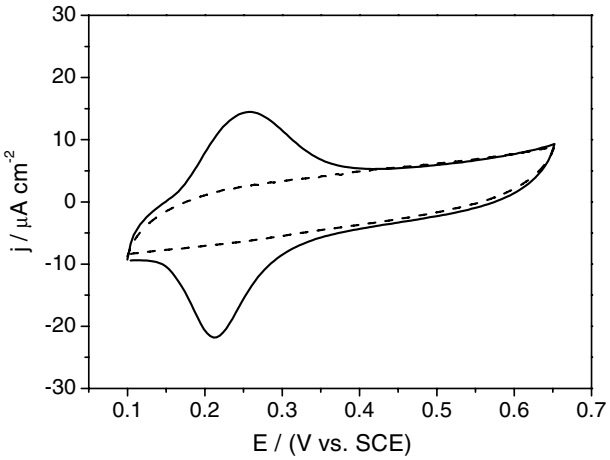


Fig. 11. Pre-concentration of $FeCO_2H$ on mixed MUA/βCDSH monolayer (full line) and the same experiment on MUA monolayer (dashed line).

Although, the defects in the βCDSH SAM were filled up with MUA, without using a protective molecule to the cyclodextrin cavity, the βCDSH SAM remained the ability to host–guest interaction with FeCOOH. Presumably, the affinity of FeCOOH was sufficient to remove the possible MUA molecules that could be in the cavity of βCDSH. This behavior can be explained by the better fitting of cyclic compounds in the cavity of β-cyclodextrin than that for acyclic guests, which prefer α-cyclodextrin [40].

Indeed, to demonstrate that the MUA modified electrode does not include $FeCO_2H$, an electrode modified only with MUA monolayer was immersed in a solution of ferrocene, in the same condition of those employed with electrode modified with mixed monolayer (Fig. 11, dashed line) and it presented no peak.

The same experiment of cyclodextrin interaction with $FeCO_2H$ molecules was carried out using a single βCDSH monolayer in order to found the additional effects of the MUA molecules in the mixed monolayer. In this sense, the βCDSH-modified gold surface was immersed in a solution of $FeCO_2H$ (1 mmol $l^{-1}$) and, transferred to supporting electrolyte solution (KCl 0.1 mol $l^{-1}$) and, finally, the cyclic voltammogram were obtained (Fig. 12).

As can be seen, the anodic peak current decreases quickly from the first up to the fourth cyclic voltammogram, which can be attributed to the leaching out of the $FeCO_2H$ molecules from the cavity of the cyclodextrin molecule. In order to verify if the decrease of the peak current of the first cycle is associated with the leach out of $FeCO_2H$ from the cyclodextrin cavity, the modified electrode was transferred to a new electrolyte solution and a new cyclic voltammogram (cycle 5) was recorded. As verified in the fifth cycle, the anodic and cathodic peak currents are not verified, indicating that the first cycle become predominantly associated to the surface bounded ferrocene by the cyclodextrin monolayer, the fourth cycle become associated fundamentally with redox process of the $FeCO_2H$ in the solution. Although the first voltammetric cycle has presented a typically adsorptive behavior for $FeCO_2H$ redox processes, the energy necessary to include

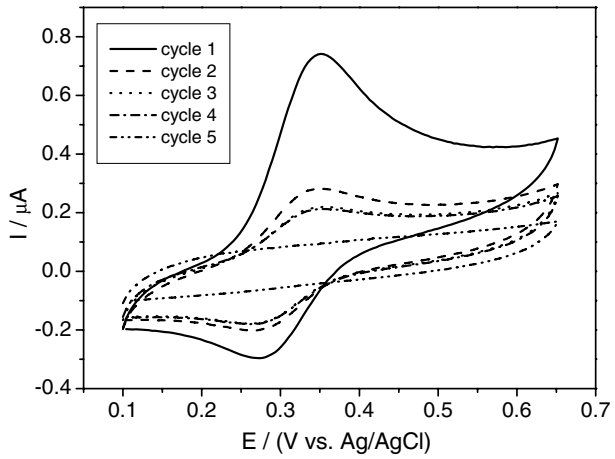


Fig. 12. Cyclic voltammograms obtained after the pre-concentration of $FeCO_2H$ on βCDSH monolayer taken in a KCl 0.1 mol $l^{-1}$ solution from first up to fourth cycle of potential (cycle 1 up to cycle 4). Cycle 5 become referring to the cyclic voltammogram to modified electrode after the carried cycle 4 in a supporting electrolyte solution without $FeCO_2H$ molecules.

ferrocenemonocarboxylic acid into the cyclodextrin cavity was similar to that referring to $FeCO_2H$ redox processes controlled by diffusion (oxidation peak was not shifted). However, can be observed an increase in the anodic peak current due to an enhancement of the electron transfer involving the adsorbed electroactive material [41].

On the other hand, the redox processes exhibited by $FeCO_2H$ molecules on mixed MUA/βCDSH monolayer behave as a typical strongly adsorbed material [41]. In this sense, the peak potential referring to cathodic and anodic processes presented behavior of pre-peaks of adsorption with peak potential negatively shifted due to the high improvement of the electron transfer due to the interaction between the βCDSH monolayer and $FeCO_2H$ molecules. This behavior can be attributed to hydrophobic alkane-like environment created by the co-adsorbed mercapto-undecanoic acid, which act favoring the host–guest complex formation. Considering the known mechanism to host–guest interaction as highly dependent on the water molecules content in the cyclodextrin cavity it is believed that the water molecule concentration at the neighborhoods of the cavity can be reduced as a result of the hydrophobic character of MUA molecules. Thus, taking account to the originally included or interacted water, the 1:1 complexation reaction of a guest (G) with a cyclodextrin host (H) may be written as follows:

$$G(gH_2O) + H(hH_2O) \leftrightarrow HG((g + h - i)H_2O) + iH_2O \quad (17)$$

where $g$ represents the number of water molecules interacting with the free guest, $h$ the number of tightly bound hydration water molecules inside the free cyclodextrin cavity, and $i$ the net displacement of the water upon complexation. As a result of a hydrophobic-like environment around of the cyclodextrin cavity, the number of water molecules situated at this interface is reduced and this equilibrium represented by Eq. (17) should shift to host–guest complex formation.

Thus, the final mixed MUA/βCDSH film presents high selectivity to ferrocenemonocarboxylic acid when compared to ferricyanide as well as the mixed-SAM of cyclodextrin showed an excellent ability to include molecules in its cavity with high stability, which opens a new field of application to these systems. The effects of surrounding groups show the great potential to design molecular architecture to mimic catalytic site of the enzymes.

## 4. Conclusions

Using the SPR and CV techniques were shown that is possible to construct self assembled monolayer of the synthesized mono(6-deoxy-6mercapto)-β-cyclodextrin able to interact with guest molecules. The SPR studies showed that βCDSH adsorbs on the gold electrode forming a film with about 60% of coverage of the surface, making necessary the use of alkyl thiol molecules to filling up the vacancies between the cyclodextrin molecules to reach the intended selectivity of the electrode. The proposed rearrange-limited model suggests that in the assembling process of this synthesized CD many molecules are adsorbed and the excess is desorbed until the adsorbed molecules become rearranged. The final mixed MUA/βCDSH film presents high selectivity to ferrocenemonocarboxylic acid when compared to ferricyanide. Indeed, the SAM of cyclodextrin shows excellent ability to include molecules in its cavity, which suggests its effective use in size-selective systems, as well as to prepare designed structure mimicking the enzyme catalytic site.

## Acknowledgements

The authors are grateful to Fundação de Amparo à Pesquisa do Estado de São Paulo (FAPESP) and Conselho Nacional de Desenvolvimento Científico e Tecnológico (CNPq) for financial support. F.S.D., R.C.S.L. and A.A.S. are indebted to FAPESP for fellowships.

## References

[1] J.L. Atwoods, J.-M. Lehn, in: J. Szejtli, T. Osa (Eds.), Comprehensive Supramolecular Chemistry, vol. 3, Pergamon, Oxford, UK, 1996, pp. 1–78.
[2] A.R. Khan, P. Forgo, K.J. Stine, V.T. D'Souza, Chem. Rev. 98 (1998) 1977–1996.
[3] J. Cszejtli, Chem. Rev. 98 (1998) 1743–1754.
[4] E.M. Martin Del Valle, Process Biochem. 39 (2004) 1033–1046.
[5] M. Singh, R. Sharma, U.C. Banerjee, Biotechnol. Adv. 20 (2002) 341–359.
[6] V.T. D'Souza, K.B. Lipkowitz, Chem. Rev. 98 (1998) 1741–1742.
[7] L. Pospisil, M.J. Svestka, J. Electroanal. Chem. 366 (1994) 295–302.
[8] M.T. Rojas, R. Koniger, J.F. Stoddart, A.E. Kaifer, J. Am. Chem. Soc. 117 (1995) 336–343.
[9] A. Ferancova, J. Labuda, W. Kutner, Electroanalysis 13 (2001) 1417–1423.

[10] D. Parker, R. Kataky, Chem. Commun. 21 (1997) 141–145.
[11] A. Ferancova, E. Korgova, R. Miko, J. Labuda, J. Electroanal. Chem. 492 (2000) 74–77.
[12] S. Busse, M. DePaoli, G. Wenz, S. Mittler, Sensors Actuat. B 80 (2001) 116–124.
[13] Y. Wang, A.E. Kaifer, J. Phys. Chem. B 102 (1998) 9922–9927.
[14] D.S. Karpovich, G.J. Blanchardt, Langmuir 10 (1994) 3315–3322.
[15] R. Subramaniam, V. Lakshminarayanan, Electrochim. Acta 45 (2000) 4501–4509.
[16] K.A. Peterlinz, R. Georgiadis, Langmuir 12 (1996) 4731–4740.
[17] C. Henke, C. Stenem, A. Janshoff, G. Steffen, H. Luftmann, M. Sieber, H.-J. Galla, Anal. Chem. 68 (1996) 3158–3165.
[18] K. Fujita, T. Ueda, T. Imoto, I. Tabushi, N. Toh, T. Koga, Bioorg. Chem. 11 (1982) 72–84.
[19] E. Kretschmann, Z. Phys. 241 (1971) 313–324.
[20] F.S. Damos, R.C.S. Luz, L.T. Kubota, Langmuir 21 (2005) 602.
[21] X. Caide, S.-F. Sui, Sensors Actuat. B 66 (2000) 174–177.
[22] K.A. Peterlinz, R. Georgiadis, Opt. Commun. 130 (1996) 260–266.
[23] H.E. Bruijn, R.P.H. Kooyman, J. Greve, Appl. Opt. 29 (1990) 1974–1978.
[24] H.E. Bruijn, B.S.F. Altenburg, R.P.H. Kooyman, J. Greve, Opt. Commun. 82 (1991) 425–432.
[25] J.C. Love, L.A. Estroff, J.K. Kriebel, R.G. Nuzzo, G.M. Whitesides, Chem. Rev. 105 (2005) 1103–1169.
[26] R.F. DeBonno, G.D. Loucks, D.D. Manna, U. Krull, Can. J. Chem. 74 (1995) 677–688.
[27] R.M.A. Azzam, N.M. Bashara, Ellipsometry and Polarized Light, Elsevier Science, Amsterdam, The Netherlands, 1977, p. 359.
[28] K. Hu, A.J. Bard, Langmuir 14 (1998) 4790–4794.
[29] T.A. Morton, D.G. Myska, I.M. Charken, Anal. Biochem. 227 (1995) 176–185.
[30] N. Camillone III, Langmuir 201 (2004) 1199–1206.
[31] Y.T. Kim, R.L. McCarley, A.J. Bard, Langmuir 9 (1993) 1941–1944.
[32] R.W. Glaser, Anal. Biochem. 213 (1993) 152–161.
[33] A.W. Adamson, Physical Chemistry of Surfaces, John Wiley & Sons, New York, 1982.
[34] A. Ulman, An Introduction to Ultrathin Organic Films, Academic Press Inc., New York, 1991.
[35] M. Dijksma, B.A. Boukamp, B. Kamp, W.P. van Bennekom, Langmuir 18 (2002) 3105–3112.
[36] G. Nelles, M. Weisser, R. Back, P. Wohlfart, G. Wenz, S. Mittler-Neher, J. Am. Chem. Soc. 118 (1996) 5039–5046.
[37] E. Sabatini, J. Rubinstein, J. Phys. Chem. 91 (1987) 6663–6669.
[38] H.O. Finklea, D.A. Snider, J. Fedyk, Langmuir 9 (1993) 3660–3667.
[39] S.-W. Choi, J.-H. Jang, Y.-G. Kang, C.-J. Lee, J.-H. Kim, Colloids Surf. A: Phys. Eng. Aspects 257 (2005) 31–36.
[40] N.V. Rekharsky, Y. Inoue, Chem. Rev. 98 (1998) 1875–1917.
[41] A. Bard, L.R. Falkner, Electrochemical Methods: Fundamentals and Applications, John Wiley & Sons, New York, 1980.